Environmental Fluid Mechanics (2020) 20:1417–1439
https://doi.org/10.1007/s10652-020-09746-6

ORIGINAL ARTICLE

Experimental analysis of flow and turbulence in the wake of neighboring emergent vegetation patches with different densities

Vasileios Kitsikoudis[1,2] · Oral Yagci[3] · V. S. Ozgur Kirca[3]

Received: 13 July 2019 / Accepted: 4 May 2020 / Published online: 14 July 2020

Abstract
Patches of vegetation in natural water bodies grow close to each other and may affect each other's wake pattern with significant implications on nutrient uptake and local sediment transport. This experimental study analyzed the wakes of two neighboring circular patches of emergent artificial vegetation with different densities, with the tested solid volume fractions being equal to 0.059, 0.114, and 0.188. The neighboring patches were positioned in two different configurations, namely side-by-side ($L/D = 0$ and $T/D = 1.5$) and staggered ($L/D = 3.5$ and $T/D = 1.5$) configurations, with D, L, and T denoting the patch diameter, the patches center-to-center longitudinal distance, and the patches center-to-center transverse distance, respectively. Results show that neighboring patches with different densities generated two distinctly different wakes at the near downstream while after 7–10D these two wakes started merging into one. The flow immediately downstream of a patch was not significantly affected by the presence of a neighboring patch and remained similar to that of an isolated patch, besides the wake of the upstream patch in staggered configuration, which was significantly affected by the downstream patch. The solid volume fraction of the neighboring patch determined the flow velocity and turbulence intensity in between the patches, which were much different compared to measurements at the side of an isolated patch.

Keywords Emergent vegetation · Flow-vegetation interaction · Neighboring vegetation patches · Shear layers · Turbulence · Wakes

✉ Vasileios Kitsikoudis
vkitsiko@civil.duth.gr

Oral Yagci
yagciora@itu.edu.tr

V. S. Ozgur Kirca
kircave@itu.edu.tr

[1] Department of Civil, Environmental, and Construction Engineering, University of Central Florida, Orlando, FL 32816, USA

[2] Present Address: Hydraulics in Environmental and Civil Engineering, Urban and Environmental Engineering, Liege University, 4000 Liege, Belgium

[3] Division of Hydraulics, Civil Engineering Department, Istanbul Technical University, 34467 Maslak, Istanbul, Turkey

1 Introduction

Vegetation is ubiquitous in natural water bodies and constitutes an essential part of sustainable ecosystems [1]. Vegetation in general improves water quality [2] and promotes biodiversity [3], riparian vegetation stabilizes banks [4], tidal marsh vegetation dictates to a large degree landscape morphodynamics through biogeomorphic feedbacks [5–8], vegetation roughness and patchiness determine hydrological connectivity in river deltas [9], and mangroves are able to attenuate long waves for shoreline protection [10]. However, vegetation is a great source of drag and flow resistance [11, 12], like many benthic organisms, e.g., [13], and can lead to reduced river conveyance capacity [14] and potentially flooding. As a result, there is a need for proper understanding of flow-vegetation interaction that will assist river management and restoration projects that aim to maintain or replace vegetation cover [15–18].

Flow-vegetation interaction has been studied extensively in recent years for a wide variety of cases, such as fully developed flows through aquatic vegetation [11], flow through isolated patches of vegetation (e.g., [19–21]), and flow through isolated tree-like floodplain vegetation (e.g., [22, 23]). The present paper focuses on the interaction of two patches of emergent vegetation, since it has been observed that vegetation patches in nature grow in close proximity to each other [24] and form irregular mosaics [25], and it is not yet clear how such an interaction affects the flow field.

Flow through and around an isolated array of circular cylinders, which is used to simulate an isolated patch of emergent vegetation, has been well documented both experimentally [20, 21, 26] and by means of numerical modeling [27, 28]. Flow that approaches such a vegetation patch gets initially decelerated and subsequently a portion of the flow gets diverted around it while another portion of the flow penetrates the porous patch. The latter is known as bleed-flow and depends on the patch density and the incoming flow velocity [20, 21]. The bleed-flow exits the patch and forms a flow region in the patch wake with low, almost constant flow velocity and suppressed turbulence [20], which promotes sediment deposition [29–31]. This region is known as the steady wake region [20, 21] and inhibits the interaction of the two shear layers that have been formed at the sides of the patch due to velocity differences. These two shear layers grow linearly until they meet at the end of the steady wake region and form a von Karman vortex street with elevated turbulence that facilitates flow recovery [21].

The coexistence of more than one vegetation patches in water bodies leads to more complex flow patterns. At reach scale, Green [32] and Nikora et al. [33] supported that total flow resistance induced by vegetation is mainly dictated by the blockage factor, which is the ratio of the channel cross-section area that is blocked by vegetation to the total cross-section. Bal et al. [34] showed that spatial distribution of vegetation patches affects flow resistance as well. In a more recent study, Luhar and Nepf [35] argued that many small patches generate greater flow resistance than a single large patch with equal channel blockage. However, they concluded that such velocity reduction is relatively small and of similar magnitude to the uncertainty introduced by the available vegetation distribution measurement techniques. In any case, the distribution of vegetation patches affects local hydrodynamics and turbulence in patch scale, which subsequently have an effect on vegetation growth and the evolution of vegetation coverage [36]. Gurnell [37] identified vegetation as an ecosystem engineer [38] that has the potential to induce biogeomorphic feedbacks by reducing flow velocity and turbulence in its near-wake region [20]. This favors entrapment of plant propagules and

establishment of seedlings [30] that promote vegetation growth. At the same time, flow gets accelerated at the sides of the patch due to flow contraction, which can even lead to local erosion, and inhibits the lateral expansion of the patch [39, 40]. The potential outcome of these two feedbacks is the downstream expansion of the vegetation patch and the formation of streamlined pioneer vegetated islands [37]. However, the presence of a neighboring vegetation patch could affect these feedbacks and alter the flow pattern that is observed downstream of an isolated vegetation patch.

While there is an abundance of studies on the interaction of two solid cylinders in tandem, side-by-side, and staggered arrangements [41, 42], there is only a limited number of studies that analyzed the hydrodynamic interaction of two vegetation patches or porous obstacles. Vandenbruwaene et al. [43] quantified how the interaction of two side-by-side patches of *Spartina anglica* affects flow contraction and argued that the acceleration in between the patches could lead to a negative feedback that will inhibit the connection of the patches, as long as the flow velocity is high enough. Meire et al. [44] also observed that the flow contraction within two side-by-side patches elevates velocity locally and resembled this pattern to a jet. They also observed a secondary zone of sediment deposition along the centerline between the patches at the point where the wakes of the two patches merge and flow velocity is diminished. They argued that if vegetation grows in this secondary area of sediment deposition, then the total vegetation drag will increase significantly, which will slow down the flow and increase sediment deposition eventually allowing the two patches to merge. Such biogeomorphic feedbacks dictate patch expansion and affect landscape evolution in larger scales [45]. de Lima et al. [46] extended the work of Meire et al. [44], by means of computational fluid dynamics, and examined how the mean flow velocity pattern changes for various positions of the neighboring patches. Yamasaki et al. [47] also analyzed numerically a flow field with randomly distributed vegetation patches and examined the evolution of vegetated landscapes based on positive and negative feedbacks (i.e., favorable or not conditions for sediment deposition and establishment of new vegetation [48]) that are induced from the interactions among patches. They showed that the complicated interaction of flow with the patches leads to increased area occupied by vegetation and that flow velocity in the unvegetated areas increases due to continuity.

Cornacchia et al. [36] tested several side-by-side and staggered configurations of patches of flexible aquatic vegetation in a field experiment and suggested that patches in a V-like formation attain the optimal combination of being exposed to small hydrodynamic forces and high nutrient availability. Cornacchia et al. [49] showed that the turbulence that is generated from an upstream dense vegetation patch and gets advected downstream can increase the nutrient uptake rate of a neighboring sparse patch located downstream. At the same time, the nutrient uptake rate of the upstream dense patch correlated well with the high mean velocities that was exposed to, highlighting the importance of spatial patch configuration in heterogeneous aquatic environments. To the best of the authors' knowledge, there have been no other studies that analyzed systematically the interaction of patches of different density, which is important since neighboring patches in nature most likely will not have the same density. The aim and novelty of the present experimental study is the analysis of the wake of two neighboring patches of emergent vegetation with equal diameter, D, but with different densities. The patches were positioned in a side-by-side and in a staggered arrangement and for each case all combinations for three different patch densities were tested.

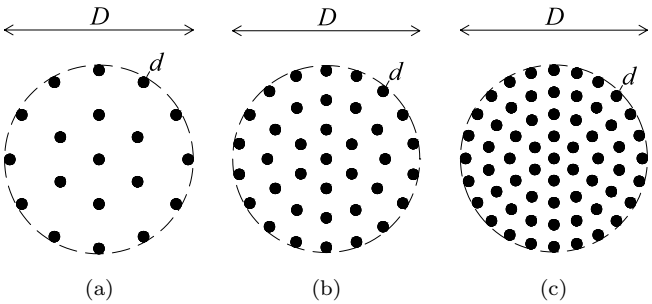

Fig. 1 Plan view of the **a** sparse, **b** medium, and **c** dense vegetation patches. Patch diameter is $D = 9$ cm and stem diameter is $d = 0.5$ cm. Flow is from left to right for each patch

Table 1 Summary of vegetation patches characteristics

Characterization	D (cm)	d (cm)	Cylinders within patch	α (m^{-1})	αD	C_D	$C_D \alpha D$	ϕ
Sparse	9	0.5	19	14.9	1.3	1	1.3	0.059
Medium	9	0.5	37	29.1	2.6	1	2.6	0.114
Dense	9	0.5	61	47.9	4.3	1	4.3	0.188

2 Methods

2.1 Experimental setup

Experiments were carried out in a recirculating flume at the Hydraulics Laboratory of Istanbul Technical University. The flume has rectangular cross-section and is 26 m long, 0.98 m wide, and 0.85 m deep, with horizontal bed from smooth concrete and Plexiglass sidewalls. A honeycomb array of small circular pipes covers the flume cross-section near the upstream end to avoid swirl and reduce turbulence of the incoming water. Flow depth is regulated by a tailgate weir at the downstream end of the flume, while two pumps were utilized to maintain the desirable flow conditions. The flume is described in more detail in [26].

Vegetation patches were simulated by circular patches of artificial vegetation represented by emergent rigid stems with circular cross-section. The patch diameter was $D = 9$ cm and the stems, which were made of steel and were coated with a very thin layer of anti-rust paint, had a diameter of $d = 0.5$ cm. The stems were arranged in a staggered configuration and three different patch densities were tested, which for simplicity will be referred as sparse, medium, and dense (Fig. 1) throughout the paper. The patch density is described by the frontal area per unit volume, $\alpha = nd$, where n is the number of stems with diameter d per unit bed area, and by the solid volume fraction, $\phi = n\pi d^2/4$ (Table 1). Chen et al. [20] analyzed the wake of such a patch based on a nondimensional flow blockage parameter, $C_D \alpha D$, where C_D is the drag coefficient, which is considered equal to one for simplicity [12]. They considered low-flow blockage as $C_D \alpha D < 4$ and high-flow blockage as $C_D \alpha D > 4$, and according to this definition, the sparse and medium patches from the

present study correspond to low-flow blockage while the dense patch to high-flow blockage (Table 1).

Flow measurements were conducted for three different experimental configurations related to the positioning of the patches (Fig. 2). The first setup comprised solely an isolated patch at the flume centerline (Fig. 2a). Such a case has been thoroughly investigated in the literature (e.g., [20, 21]); however, the wake of an isolated patch is also analyzed herein as a reference case to compare with the wake of the same patch when it is affected by a neighboring patch. The second experimental setup consisted of two vegetation patches in side-by-side configuration (Fig. 2b) and the third one comprised two patches in staggered configuration (Fig. 2c). The longitudinal spacing of the centers of the two patches, L, is zero for the side-by-side and $3.5D$ for the staggered experimental setup. In the transverse direction, the distance between the two neighboring patch centers, T, is $1.5D$, or alternatively the transverse gap separating the two patches is $0.5D$, both for the side-by-side and staggered configurations. The two patches were equally spaced from the flume centerline in the transverse direction.

2.2 Flow velocity measurements and data post-processing

Three-dimensional flow velocity measurements were conducted with a downlooking Nortek Vectrino Profiler at points across the horizontal plane mid-depth in the patches wake (Fig. 2), similar to [20, 21, 44]. The Vectrino was mounted on a custom-made rolling platform, which allowed the accurate positioning of the instrument. Measurements were denser close to the patches to properly capture the steep velocity gradient due to flow-body interaction. No measurements were conducted close to the upstream patch in the staggered setup (Fig. 2c) because the bulky supporting elements that were keeping the patches in place did not allow the proper positioning of the Vectrino. The flow field downstream of isolated patches and side-by-side patches with same density was considered to be

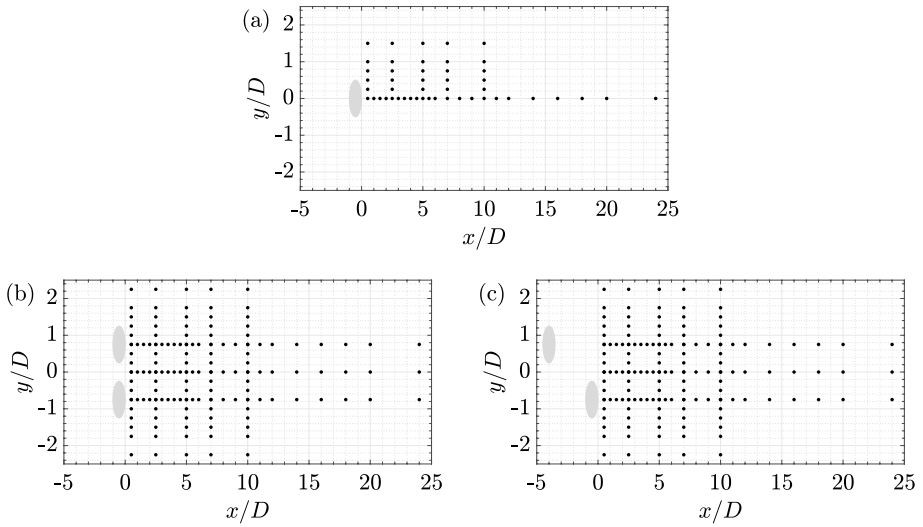

Fig. 2 Grid of flow velocity point measurements at the horizontal plane mid-depth for flow through **a** an isolated patch, **b** side-by-side patches, and **c** staggered patches. Flow is from left to right

symmetric around the flume centerline and measurements were conducted only at half of the flume width.

Water for the flume was supplied by an adjacent lake, which had an abundance of suspended particles that facilitated the Doppler shift and secured high correlation and signal-to-noise ratio, with mean values greater than 95% and 30 dB, respectively, for reliable measurements. The sampling volume was located 5 cm below the probe transceiver, where the geometry of the Vectrino probe offers the most accurate measurements [50]. At each point of the measurements grid (Fig. 2), flow velocity was recorded for 100 s with 100 Hz sampling rate. Mori et al. [51] showed that high-quality statistics do not always guarantee the exclusion of outliers from the data. A few outliers in the obtained time-series were detected with the phase-space thresholding methodology of Goring and Nikora [52] as modified by Wahl [53], and replaced with cubic polynomial interpolation. All experiments were conducted with steady flow conditions, with 30 cm flow depth and mean approaching flow velocity, U_0, equal to 24.4 ± 0.3 cm/s (mean $\pm$ one standard deviation). U_0 was measured far upstream from the patches, at mid-depth, at a location that was not affected by the presence of the patches and where fully developed turbulent flow was observed.

The measured flow velocities are denoted as u, v, and w for the longitudinal, x, transverse, y, and vertical, z, direction, respectively. Instantaneous velocities consist of a time-averaged ($\overline{u}$, $\overline{v}$, $\overline{w}$) and a fluctuating (u', v', w') component, according to Reynolds decomposition (e.g., $u = \overline{u} + u'$, for the longitudinal flow velocity). The standard deviation of a steady flow velocity time-series expresses statistically the turbulence intensity, as defined by $\sqrt{\overline{u'^2}}$, $\sqrt{\overline{v'^2}}$, and $\sqrt{\overline{w'^2}}$ for each direction. Turbulent kinetic energy (TKE) per unit mass, k, is defined from the following equation [54]:

$$k = \frac{1}{2}(\overline{u'^2} + \overline{v'^2} + \overline{w'^2}) \tag{1}$$

3 Results and discussion

3.1 Flow in the wakes of the patches

In this section, the results will be analyzed by keeping the density of one of the patches as medium and varying the density of the neighboring patch. Three different cases will be examined, with the medium patch being: (1) the upstream patch in staggered arrangement (Sect. 3.1.1, Fig. 2c), (2) the downstream patch in staggered arrangement (Sect. 3.1.2, Fig. 2c), and (3) one of the two patches in side-by-side arrangement (Sect. 3.1.3, Fig. 2b). In every case, the density of the neighboring patch will vary from sparse to medium to dense.

3.1.1 Two patches in staggered arrangement: influence of the downstream patch on the wake of the upstream patch

When the medium density patch is placed at the upstream position in the staggered arrangement, it can be observed that the neighboring patch alters radically its wake compared to the wake of the isolated medium density patch (Fig. 3a, d). An isolated medium patch exhibits a well-defined steady wake region with low mean velocity (Fig. 3a) and turbulence (Fig. 3d). After the end of the steady wake region, the velocity increases rapidly towards

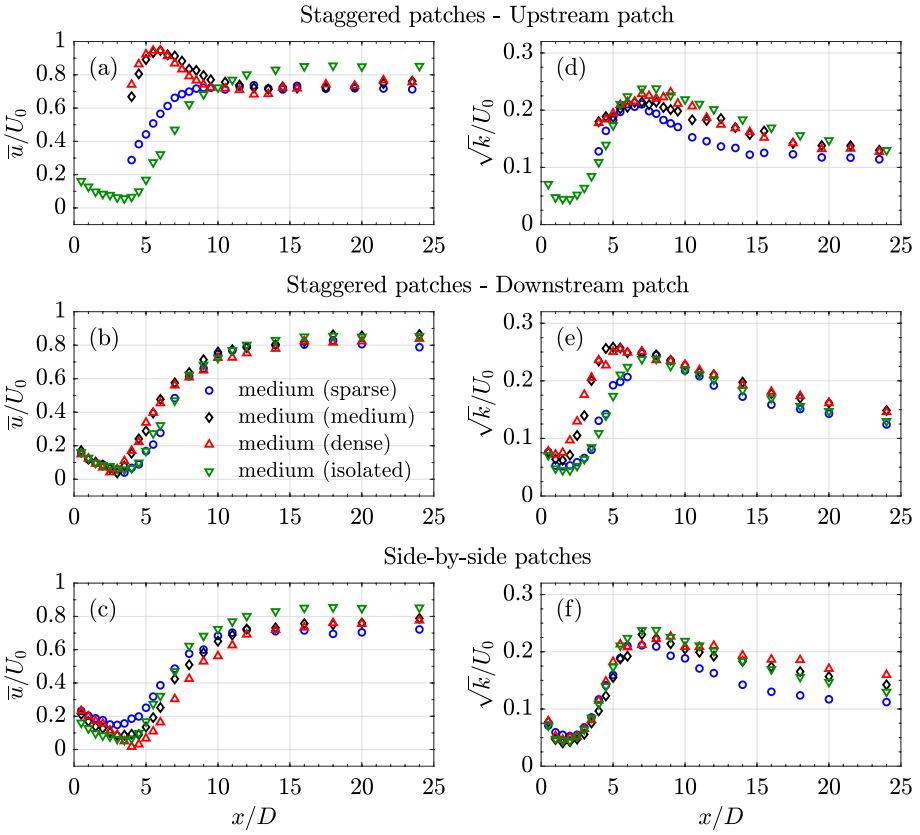

Fig. 3 Profiles of normalized mean longitudinal velocity, $\overline{u}/U_0$, along the longitudinal axis downstream of a medium patch when it is **a** upstream patch of two patches in staggered arrangement, **b** downstream patch of two patches in staggered arrangement, and **c** one of the two patches in side-by-side arrangement. Similarly for normalized square-root turbulent kinetic energy, $\sqrt{k}/U_0$, in **d**–**f**. The downstream edge of the patches is located at $x/D = 0$. The legend shows in parentheses the density of the patch that is neighboring to the medium patch

flow recovery due to intense mixing and the formation of a patch-scale von Karman vortex street [20, 21], which is manifested by a peak in TKE, 8D downstream of the isolated medium patch (Fig. 3d). Although no velocity measurements were conducted down to 4D from the rear edge of the upstream patch in staggered arrangement, it can be inferred from Fig. 3a that the steady wake region behind the upstream patch is significantly shortened in the presence of a downstream patch. The portion of the flow that is diverted by the downstream patch accelerates the flow in the wake of the upstream patch, with the density of the downstream patch influencing significantly this process (Fig. 4).

The influence of the sparse downstream patch on the wake of the medium upstream patch leads to a longitudinal velocity profile that is fairly similar to the isolated medium patch; however, the velocity increases at a shorter distance (Fig. 3a). When the neighboring patch is the medium or dense one, it leads to a much different flow pattern such that the velocity gets increased up to almost the undisturbed value U_0 at 6D, and afterwards gets reduced (Fig. 3a). The initial sharp velocity increase is owed to the increased density

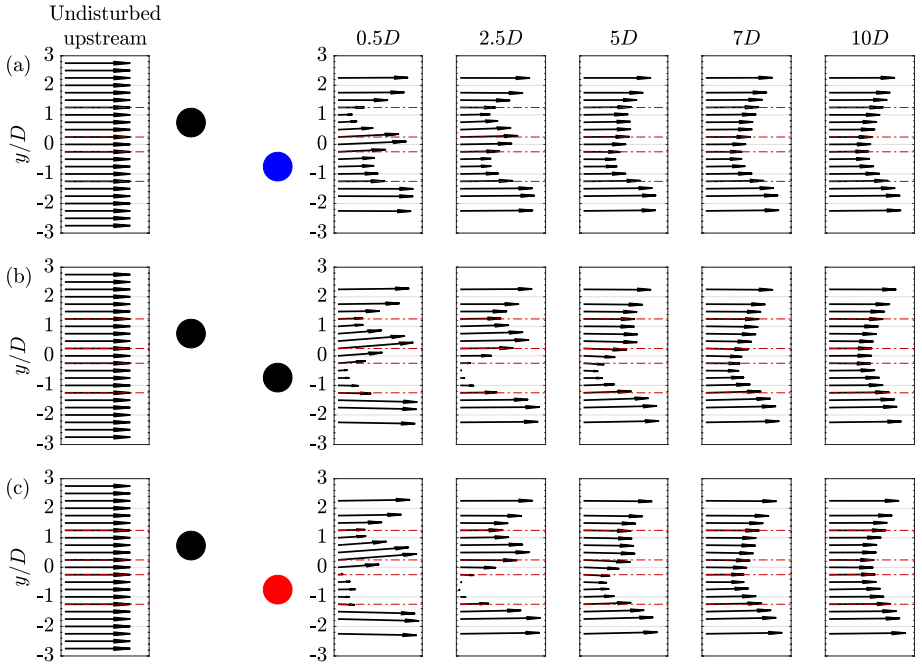

Fig. 4 Vectors of mean horizontal velocity for staggered patches with a medium density patch located upstream and a **a** sparse, **b** medium, and **c** dense patch located downstream. Upstream and downstream patches are positioned at $y/D = [1.25\ 0.25]$ and $y/D = [-0.25\ -1.25]$, respectively, as denoted by red dash-dotted lines. The blue, black, and red circles denote a sparse, medium, and dense patch, respectively. The downstream distances 0.5, 2.5, 5, 7, and 10D shown in **a** are with respect to the rear edge of the downstream patch (Fig. 2c)

of the downstream patch, which enhances the flow contraction. The subsequent velocity reduction from 6D and further downstream is due to the merger of the individual wakes of the upstream and downstream patches into one (Fig. 5a). The velocity in the wake of the upstream medium patch is considerably greater than the velocity in the wake of the downstream medium or dense patch and a steep velocity gradient is formed (Fig. 5a). This leads to enhanced shear (Fig. 5c) and elevated turbulence (Fig. 5b), especially from 6D to 10.5D in between the wakes of the downstream and the upstream patch.

From Figs. 4 and 5, it can be seen that the transverse velocity gradients at the two sides of the wake of the upstream patch are not the same due to the additional flow contraction that is induced by the downstream patch at one of the sides. As a result, the shed vortices from the two sides of the upstream patch are expected to be uneven and of different magnitude. This asymmetry is likely to cause a disruption in the formation of a well-defined von Karman vortex street, as can be inferred by examining the power spectral densities of transverse velocities at the point of maximum TKE for the isolated medium patch at 8D (Fig. 6a). For the isolated medium patch there is a distinguishable peak at around 0.5 Hz, which flattens in the wake of the upstream patch (Fig. 6a). The resemblance of the vortex shedding mechanism of the medium porous patch to that of a solid cylinder of equal overall diameter, D, can be examined with the aid of Strouhal number, which is defined as $St = f_D D/U_0$, where f_D is the shedding frequency. For a solid cylinder

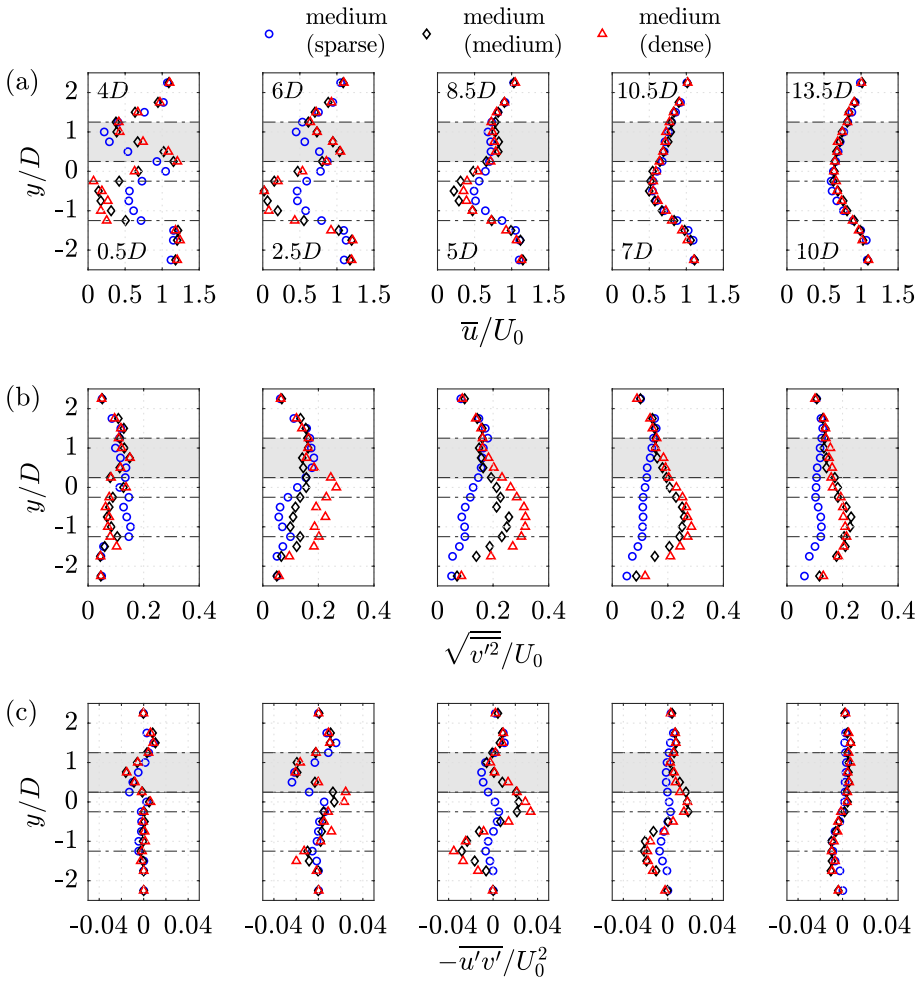

Fig. 5 Transverse profiles of normalized **a** mean longitudinal velocity, $\overline{u}/U_0$, **b** transverse turbulence intensity, $\sqrt{\overline{v'^2}}/U_0$, **c** Reynolds shear stress, $-\overline{u'v'}/U_0^2$, downstream of vegetation patches in staggered arrangement. The legend shows in parentheses the density of the patch that is neighboring to the medium patch, which is held constant at the upstream position. The gray shaded area in between the dashed lines at $y/D = [0.25\ 1.25]$ shows the position of the upstream medium patch and the dashed lines at $y/D = [-1.25\ -0.25]$ show the position of the neighboring patch. The downstream distances shown at the top (4, 6, 8.5, 10.5, and 13.5D) and the bottom (0.5, 2.5, 5, 7, and 10D) of the subfigures in **a** are with respect to the rear edge of the upstream and downstream patch (Fig. 2c), respectively

with diameter of 9 cm (i.e., equal to the patch diameter), the cylinder Reynolds number is $Re_D = U_0 D/\nu = 22{,}000$, where ν is the kinematic viscosity of water, and the Strouhal number should be approximately 0.20 [55]. The shedding frequency that is derived from this Strouhal number is $f_D = U_0 St/D = 0.54$ Hz, which agrees well with the observed peak frequency of the medium patch.

Figure 5c shows that 8.5D downstream of the upstream patch, the longitudinal flux of transverse turbulent momentum, as expressed by the horizontal Reynolds shear stress $-\overline{u'v'}/U_0^2$, is much different at the two sides of the wake of the upstream medium patch when

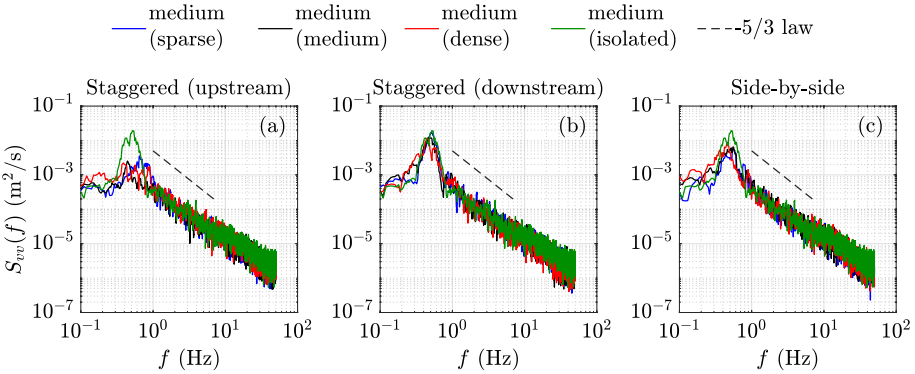

Fig. 6 Power spectral densities measured at $8D$ downstream of a medium patch, i.e., at the point where maximum $\sqrt{\overline{v'^2}}/U_0$ is observed for the isolated medium patch, when it is **a** the upstream patch of two patches in staggered arrangement, **b** the downstream patch of two patches in staggered arrangement, and **c** one of the two patches in side-by-side arrangement. The legend shows in parentheses the density of the patch that is neighboring to the medium patch

the downstream patch is the medium or the dense one. Specifically, the side of the wake that faces the neighboring patch (i.e., at $y/D = 0.25$) exhibits much greater $-\overline{u'v'}/U_0^2$ values compared to the opposite side of the patch (i.e., at $y/D = 1.25$). When the downstream neighboring patch is the sparse one, this effect is diminished and the Reynolds shear stresses at the two sides of the wake of the upstream patch are similar. Figure 5b shows a similar pattern for the transverse turbulence intensities, which is more persistent than that of the shear stresses and extends farther downstream.

The alteration of the pattern of turbulence in the wake of the upstream patch becomes more evident by examining the joint frequency distributions (JFDs) of the longitudinal and transverse turbulence fluctuations, normalized with the respective turbulence intensity, at the point where maximum TKE was observed downstream of an isolated medium patch, i.e., at $8D$ (Fig. 7). The JFD of the isolated patch exhibits a distinct bimodal distribution (Fig. 7a), quite similar to what is observed downstream of a solid upright cylinder [56] due to the oscillating nature of vortex shedding. When the medium patch has a downstream neighboring patch of medium or dense density in staggered arrangement, the JFD pattern becomes radically different and uncorrelated (Fig. 7c, d). For the sparse neighboring patch, the longitudinal and transverse turbulence fluctuations in the wake of the upstream medium patch appear to be positively correlated (Fig. 7b). Despite these, the TKE profiles along the patchline remain relatively similar to the isolated medium patch (Fig. 3d).

The findings of this section agree with the numerical studies of de Lima et al. [46] and Yamasaki et al. [47], who also showed that the downstream patch of neighboring patches in staggered arrangement can increase the flow velocity in the wake of the upstream patch and maintain sediment in suspension. Particularly, de Lima et al. [46] showed that such an interaction between two staggered patches may occur up until $L/D = 6$. Herein, the tested longitudinal distance between the patches was $L/D = 3.5$ (Fig. 2c).

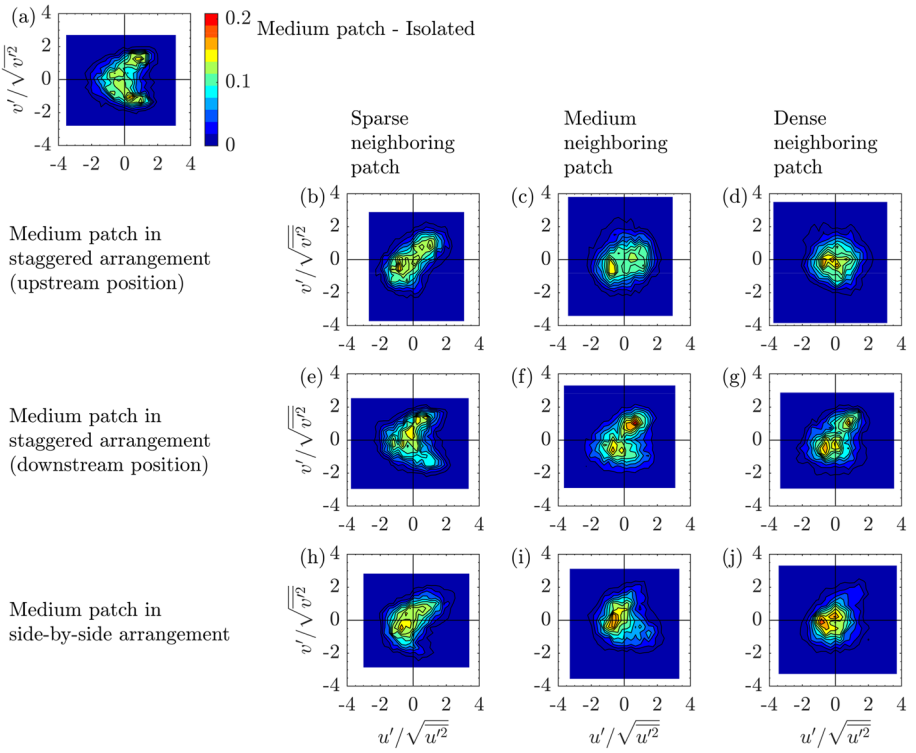

Fig. 7 Joint frequency distributions of normalized longitudinal velocities, $u'/\sqrt{\overline{u'^2}}$, and transverse velocities, $v'/\sqrt{\overline{v'^2}}$, $8D$ downstream of a medium patch, i.e., at the point where maximum $\sqrt{\overline{v'^2}}/U_0$ is observed for the isolated medium patch

3.1.2 Two patches in staggered arrangement: influence of the upstream patch on the wake of the downstream patch

Contrary to the upstream patch, the mean velocity in the wake of the downstream patch in staggered arrangement is hardly affected by the presence of a neighboring patch (Fig. 3b). TKE along the patch centerline is not particularly affected either when the neighboring patch is the sparse one. However, for medium and dense neighboring patches the peak of patch scale turbulence extends towards the patch (Fig. 3e), shortening the steady wake region behind the patch. The peak in power spectral densities, $8D$ downstream of the medium patch, remains similar to that of an isolated medium patch and is not affected by the presence of the upstream patch, regardless of the density (Fig. 6b). However, the JFD shows that the bimodal pattern of the isolated patch gets distorted due to the asymmetry as the density of the upstream patch increases (Fig. 7e–g). This is due to the fact that the turbulence generated from the upstream patch influences the patch-scale turbulence of the downstream patch. This is evident from Fig. 8, where it can be seen that while the normal and shear Reynolds stress transverse profiles $0.5D$ downstream of a downstream medium patch with a neighboring upstream patch are almost identical to that $0.5D$ downstream of

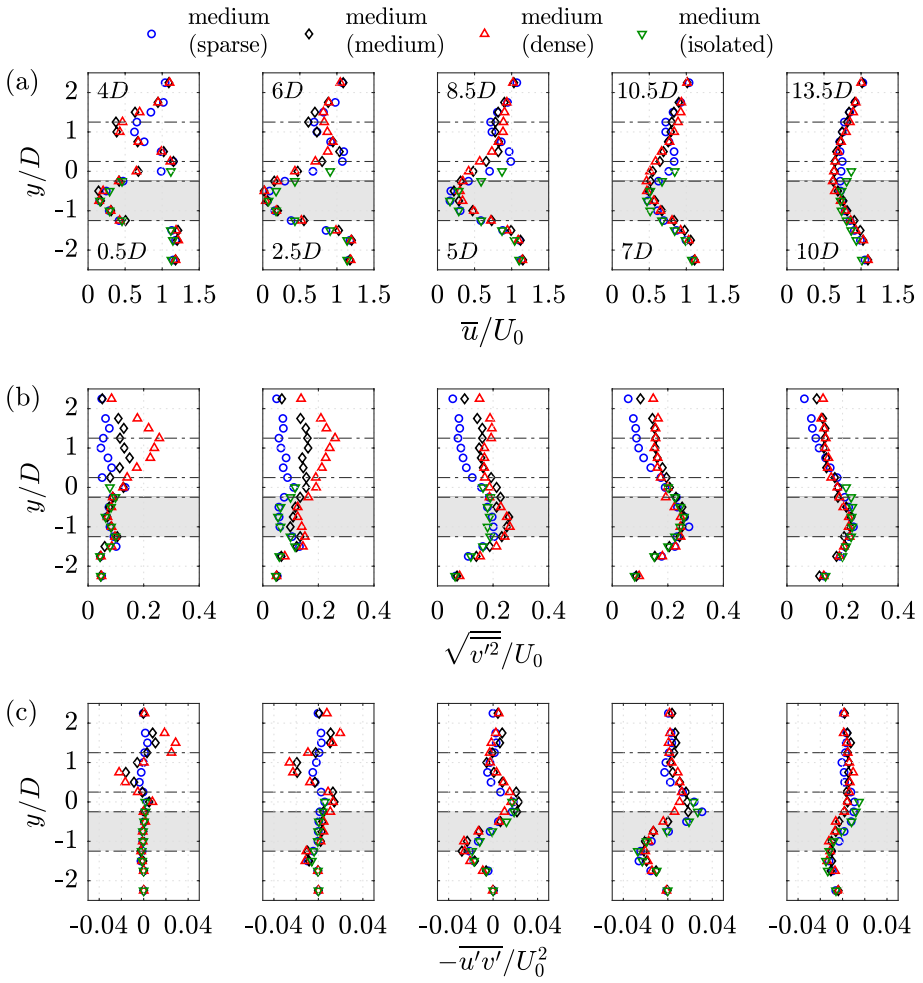

Fig. 8 Transverse profiles of normalized **a** mean longitudinal velocity, $\overline{u}/U_0$, **b** transverse turbulence intensity, $\sqrt{\overline{v'^2}}/U_0$, **c** Reynolds shear stress, $-\overline{u'v'}/U_0^2$, downstream of vegetation patches in staggered arrangement. The legend shows in parentheses the density of the patch that is neighboring to the medium patch, which is held constant at the downstream position. The gray shaded area in between the dashed lines at $y/D = [-1.25\ -0.25]$ shows the position of the downstream medium patch and the dashed lines at $y/D = [0.25\ 1.25]$ show the position of the neighboring patch. The downstream distances shown at the top (4, 6, 8.5, 10.5, and 13.5D) and the bottom (0.5, 2.5, 5, 7, and 10D) of the subfigures in **a** are with respect to the rear edge of the upstream and downstream patch (Fig. 2c), respectively

the isolated medium patch, the cases where the upstream neighboring patch is of medium or dense density get differentiated from 2.5D to 7D. This implies that the flow penetrating the downstream patch is similar for all cases; however, its wake is affected by the wake of the upstream patch.

The small alteration of TKE in the wake of the medium patch at the downstream position stimulated a similar analysis for the wake of a sparse patch in the same position, which has a longer steady wake region due to enhanced bleed-flow. It can be observed in Fig. 9 that while mean longitudinal velocity remains similar in all cases, TKE increases

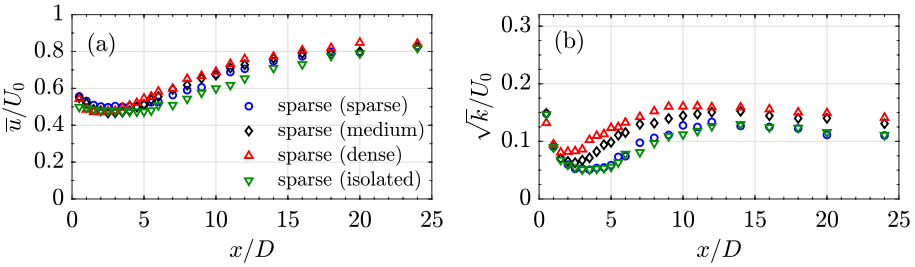

Fig. 9 Profiles of **a** normalized mean longitudinal velocity, $\overline{u}/U_0$ and **b** normalized turbulent kinetic energy, $\sqrt{k}/U_0$ along the longitudinal axis downstream of a sparse patch when it is the downstream patch of two patches in staggered arrangement. The downstream edge of the downstream patch is located at $x/D = 0$ (Fig. 2c). The legend shows in parentheses the density of the neighboring patch that is located upstream of the sparse patch

substantially in the presence of a medium or dense neighboring upstream patch. A sparse neighboring patch has no substantial effect. The enhancement of turbulence in the steady wake region of the downstream patch has potential implications on sediment and propagule deposition, since elevated turbulence levels can maintain particles in suspension.

3.1.3 Two patches in side-by-side arrangement: influence of the neighboring patch on the wake of a patch of medium density

For patches in side-by-side arrangement, the mean velocity along the patch centerline in the wake of the medium patch is not substantially influenced by a neighboring patch (Figs. 3c, 10), which agrees with the findings of Meire et al. [44]. Only the sparse neighboring patch induces slightly higher velocities near the patch within the steady wake region (Fig. 3c). TKE exhibits two distinct peaks, similar to an isolated patch (Fig. 3f). The first peak, immediately downstream of the patch, is induced by individual stem generated turbulence and the second is due to patch scale turbulence [20], with both of them remaining relatively invariant with changing density of the neighboring patch in side-by-side arrangement (Fig. 3f). The JFDs of side-by-side arrangements indicate that the von Karman vortex street downstream of a patch with a side-by-side neighbor (Fig. 7h–j) is not as well organized as that of an isolated patch (Fig. 7a) given that the velocity gradients at the two sides of the patch are different (Fig. 10a), causing the vortices to be asymmetric. This change also manifests itself by the reduction in the peaks of power spectral densities in Fig. 6c.

3.2 Flow in between the patches and merger of the wakes of neighboring patches

In this section, results for flow in between the neighboring patches and the associated momentum transfer are compared by examining all possible combinations of patch densities for the side-by-side configuration (Sect. 3.2.1, Fig. 2b) and for the staggered configuration when the downstream patch is held constant (Sect. 3.2.2, Fig. 2c).

3.2.1 Flow in between patches in side-by-side configuration

Meire et al. [44] considered the flow in between two patches of same density in side-by-side arrangement to be similar to a turbulent jet, when the patches are close enough to affect each

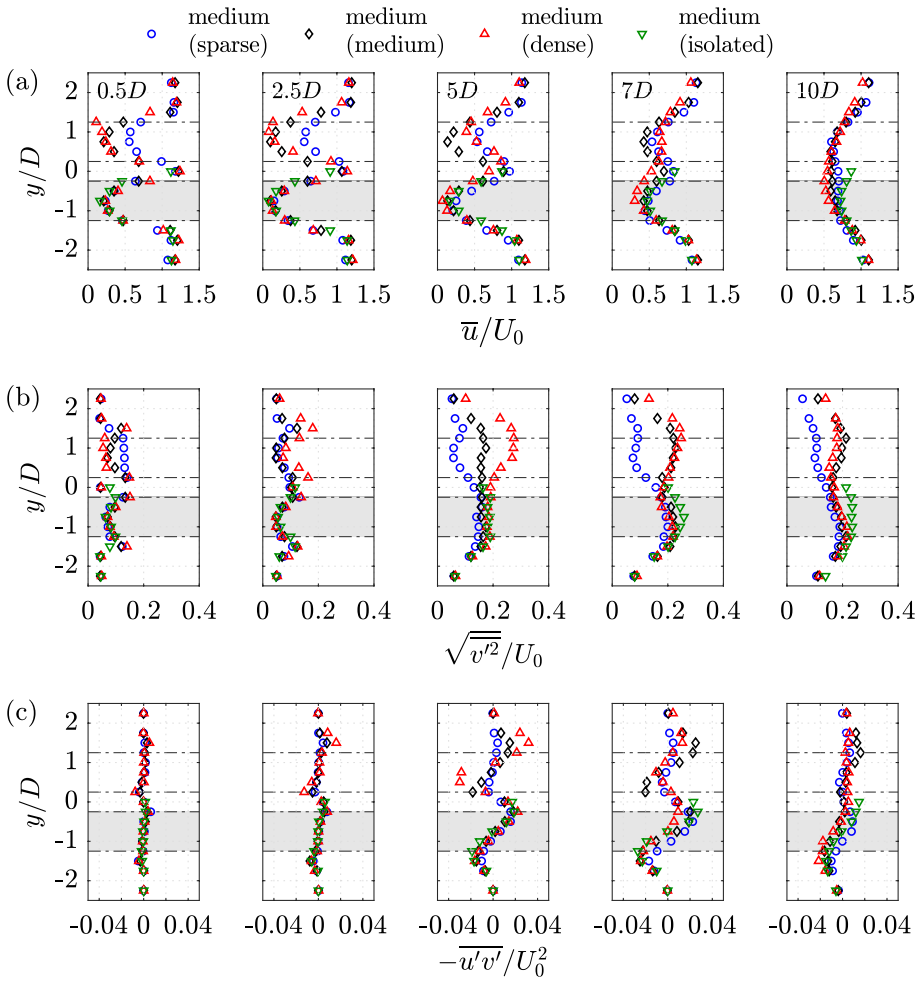

Fig. 10 Transverse profiles of normalized **a** mean longitudinal velocity, $\overline{u}/U_0$, **b** transverse turbulence intensity, $\sqrt{\overline{v'^2}}/U_0$, **c** Reynolds shear stress, $-\overline{u'v'}/U_0^2$, downstream of vegetation patches in side-by-side arrangement. The legend shows in parentheses the density of the patch that is neighboring to the medium patch. The gray shaded area in between the dashed lines at $y/D = [-1.25 \ -0.25]$ shows the position of the medium patch and the dashed lines at $y/D = [0.25 \ 1.25]$ show the position of the neighboring patch. The downstream distances 0.5, 2.5, 5, 7, and 10D shown in **a** are with respect to the rear edge of the patches (Fig. 2b)

other. In such a case, the longitudinal velocity is increased in between the patches to satisfy continuity and two shear layers are formed immediately downstream of the patches due to velocity difference between the induced jet and the slower moving water at the near wake region behind each patch. Normalized mean longitudinal velocity profiles given in Fig. 11 show that when patch density is kept constant for one of the two patches in side-by-side arrangement, increasing density of the neighboring patch initially elevates the longitudinal flow velocity in between the patches and leads to a lower minimum velocity further downstream. The initial increase in velocity in between the patches for denser neighboring patch

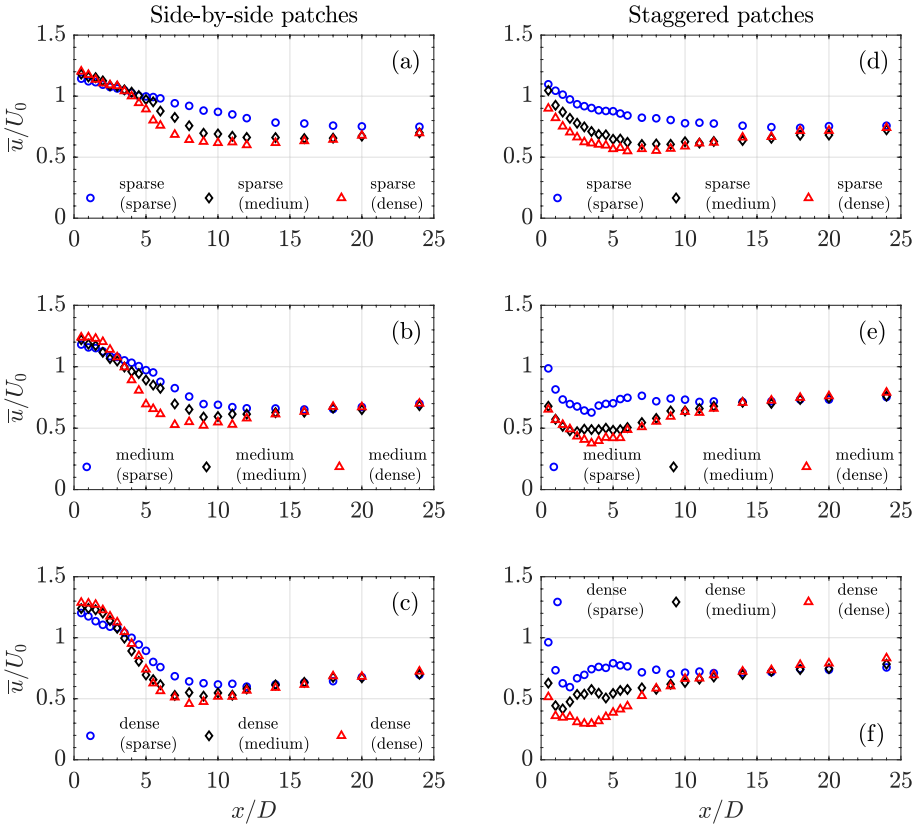

Fig. 11 Normalized mean longitudinal velocity, $\overline{u}/U_0$, along the longitudinal axis in between the patches. All possible combinations for side-by-side arrangement with respect to the **a** sparse, **b** medium, and **c** dense patch, and for staggered arrangement with respect to the downstream **d** sparse, **e** medium, and **f** dense patch. For patches in side-by-side configuration, the downstream edge of the patches is located at $x/D = 0$ (**a**–**c**) (Fig. 2b) while for patches in staggered configuration, the downstream edge of the downstream patch is located at $x/D = 0$ (**d**–**f**) (Fig. 2c). Legend shows the density of the patch that is held constant and in parenthesis the density of the neighboring patch

is an obvious effect of enhanced flow contraction, since a dense patch diverts laterally a larger portion of the flow compared to a sparse patch. Additionally, the flow in between the patches is enhanced by the flow that gets diverted by the neighboring patch.

Further downstream, the near wake flow characteristics of each patch affect the lateral momentum exchange between the patch wakes and the jet in between the patches. For side-by-side patches with equal density, lateral turbulent mixing occurs at the same rate at both sides of the jet due to symmetry. However, in nature it is rather unlikely that two neighboring patches will have exactly the same density. As a result, the velocity in their wakes will be different and the momentum of the induced jet will be dissipated at different rates at its sides. The effect of this asymmetry around the jet is mostly visible in Fig. 11a, which shows the mean longitudinal velocity profile along the axis in between side-by-side patches when the sparse patch is held constant. It can be observed that close to the patches, flow velocity gets reduced at a similar rate for every density of the neighboring patch. However, at $4D$ downstream of the patches the velocity gradient gets steeper as the neighboring

patch density increases. This is owed to the fact that the lateral shear layers have grown and started to dissipate the momentum of the jet at different rates due to variations in shear layer thickness and velocity difference between the jet and the near wake region of each patch. The denser the neighboring patch, the steeper the velocity gradient becomes and the lateral mixing is enhanced. This leads to lower minimum velocities for denser patches. The two individual wakes of the two patches eventually merge and form a unified wake, with the velocity at the centerline at $10D$ downstream of the patches being considerably lower than the velocity observed at the side of an isolated patch (Fig. 10a).

Different flow patterns are expected for the tested arrangements when comparing the mean longitudinal velocity along the axis in between the patches, $\overline{u}_{np}$, to the mean longitudinal velocity at a transverse distance of $0.25D$ from the lateral edge of an isolated patch, $\overline{u}_{is}$. For the side-by-side patches, $\overline{u}_{np}$ is initially greater than $\overline{u}_{is}$ until 2.5–5D downstream of the patches, with the difference becoming more notable with increasing density of the neighboring patch (Fig. 12a–c) and enhanced flow contraction. Afterwards, $\overline{u}_{np}$ becomes

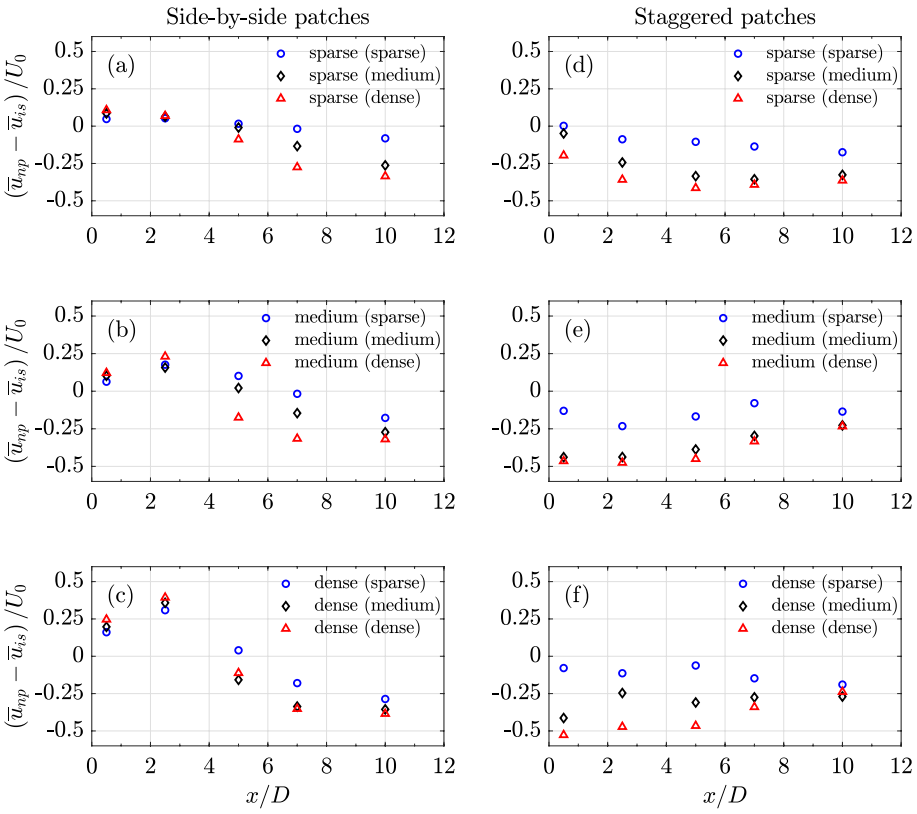

Fig. 12 Relative difference of mean velocity along the longitudinal axis in between neighboring patches, $\overline{u}_{np}$, and mean velocity from respective points with transverse distance $0.25D$ from the edge of an isolated patch, $\overline{u}_{is}$, with same density. All possible combinations for side-by-side arrangement with respect to the **a** sparse, **b** medium, and **c** dense patch, and for staggered arrangement with respect to the **d** sparse, **e** medium, and **f** dense downstream patch. For patches in side-by-side configuration, the downstream edge of the patches is located at $x/D = 0$ (**a–c**) (Fig. 2b) while for patches in staggered configuration, the downstream edge of the downstream patch is located at $x/D = 0$ (**d–f**) (Fig. 2c). Legend shows the density of the patch that is held constant and in parenthesis the density of the neighboring patch

lower than $\overline{u}_{is}$, with increasing density of the neighboring patch again amplifying the difference, but this time showing the merger of the two neighboring patch wakes into one. In general, the difference of these two variables, $\overline{u}_{np} - \overline{u}_{is}$, ranges from $0.05U_0$ to $-0.08U_0$ when a sparse patch has a sparse side-by-side patch, and from $0.39U_0$ to $-0.39U_0$ when a dense patch is placed side-by-side to another dense patch.

The presence of a side-by-side patch alters both the maximum value of TKE along the axis in between the patches and the point where this occurs (Fig. 13). Specifically, TKE increases with increasing density of the neighboring patch, while its peak is shifted downstream with decreasing density of the neighboring patch. This can be associated with patch scale turbulence and the strengthening of lateral turbulent mixing due to formation of a von Karman vortex street behind each patch, which can affect the flow beyond the patch transverse width [44]. The required distance for the interaction of the two shear layers that are formed at the sides of an isolated patch is longer for sparse compared to dense patches [20, 26]. The enhanced lateral mixing that occurs in side-by-side patches eventually leads to the

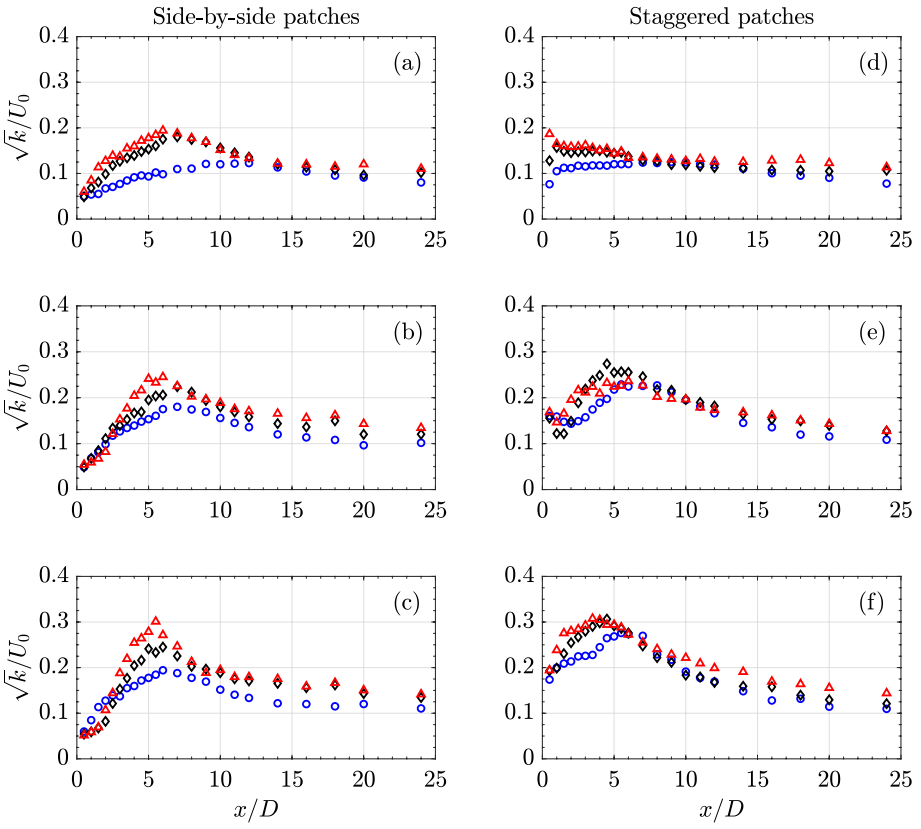

Fig. 13 Normalized square-root turbulent kinetic energy, $\sqrt{k}/U_0$, along the longitudinal axis in between the patches. All possible combinations for side-by-side arrangement with respect to the **a** sparse, **b** medium, and **c** dense patch, and for staggered arrangement with respect to the downstream **d** sparse, **e** medium, and **f** dense patch. For patches in side-by-side configuration, the downstream edge of the patches is located at $x/D = 0$ (**a**–**c**) (Fig. 2b) while for patches in staggered configuration, the downstream edge of the downstream patch is located at $x/D = 0$ (**d**–**f**) (Fig. 2c). Legend is same with Fig. 11

formation of a single wake and reduced longitudinal mean velocities and Reynolds stresses at $x/D = 7-10$, when compared to measurements at the same lateral distance from the side edge of an isolated patch with same density (Fig. 10).

Flow through side-by-side solid circular cylinders has been analyzed thoroughly and has been observed that for $T/D > 2.2$ two parallel von Karman vortex streets are formed while for $T/D < 1.2$ the two cylinders act as a single bluff body forming a single von Karman vortex street [41]. In between these thresholds, the wake of the two cylinders is asymmetric with the flow exiting the gap being biased towards one of the individual wakes, reducing the wake length and increasing the vortex shedding frequency of one cylinder compared to the neighboring cylinder [41]. For side-by-side porous obstacles ($L/D = 0$), such as those tested herein, Meire et al. [44] observed that such biased flow occurred only when the two patches were connected, i.e., for $T/D = 1$. When the two patches were not connected, they observed flow acceleration in between circular patches for $T/D \leq 1.63$. In their numerical study, de Lima et al. [46] noted that when $T/D > 1.25$ for side-by-side patches, the wake of each patch is similar to that of the corresponding isolated patch. Vandenbruwaene et al. [43] observed that squared patches of *Spartina anglica* in side-by-side arrangement begin to interact from approximately $T/D = 3.3$ up until $T/D = 1.1$ at which point the two patches act as one. They observed that in between these two limits the flow gets accelerated and argued that this should lead to a negative feedback that hinders the lateral expansion of the patch, provided that the incoming velocity is high enough. Their findings were also validated for patches with circular shape. In the present study *T/D* was set equal to 1.5 and it was observed that flow in between the patches was much different than flow around an isolated patch (Fig. 12), which means that the patches interacted with each other.

Meire et al. [44] observed in their experiments that the flow velocity in between side-by-side patches was initially steady along a region that is called the potential core [57] and after the lateral shear layers had grown enough to affect the centerline velocity, the velocity decreased towards a minimum, which signified the merger of the wakes of the two patches into one single wake. A potential core was not observed in the present study but instead, velocity started to decrease immediately from the first measurement point, $0.5D$ downstream of the patches (Fig. 11a-c). When compared to the experiments of Meire et al. [44], the absence of a potential core region could be attributed to enhanced turbulence that is generated from the significantly greater incoming velocity herein, which was equal to 24.4 ± 0.3 cm/s, which is almost 2.5 times greater than that of Meire et al. [44]. Enhanced turbulence presumably facilitates turbulent mixing and could lead to faster dissipation of the momentum of the jet. A relevant observation was made by Meire et al. [44] who observed much greater values of the kinematic spreading coefficient (i.e., deceleration occurred at a faster rate) compared to values for free planar turbulent jets from the literature and attributed this difference to elevated turbulence. Finally, the diameter of the porous obstacles herein was 9 cm, which is much smaller than the 22 cm wide patches used in [44] and as a result the flow contraction was different.

3.2.2 Flow in between patches in staggered configuration

The mean normalized longitudinal velocities along the axis in between patches in staggered arrangement also depend on the density of the neighboring patch. When the downstream patch density is kept constant, the density of the upstream patch dictates to a large degree the longitudinal $\overline{u}/U_0$ profile along the flume centerline. For example, at the first measurement point at $0.5D$ downstream of the downstream patch, or alternatively $4D$

downstream of the upstream patch (Fig. 2c), the $\overline{u}/U_0$ velocity is always higher when the upstream patch is the sparse one, followed by the medium and dense patches (Fig. 11d–f). This is the opposite trend to that observed for side-by-side patches (Fig. 11a–c). The minimum attained values are lower when the downstream patch is influenced by the dense patch, followed by the medium and sparse patches, which is in agreement with the side-by-side patches.

When considering the difference between the velocity in between patches in staggered arrangement and the velocity at the side of an isolated patch, it can be deduced that the latter is greater (Fig. 12d–f). This difference increases with downstream distance when the sparse patch is considered at the downstream position of the staggered configuration and decreases with distance or remains invariant when the medium and dense patches are kept constant at the downstream position. Similarly to the side-by-side patches, the density of the neighboring patch (i.e., the upstream one in this case) dictates the difference between the velocity in between the patches and the velocity at the side of an isolated patch, with denser patches increasing the difference. In fact, the density of the neighboring patch appears to be more influential in staggered arrangement than in side-by-side arrangement.

The normalized TKE profiles along the axis in between patches in transverse configuration have some differences compared to the respective profiles for side-by-side patches (Fig. 13). Specifically, the $\sqrt{k}/U_0$ values at the first measurement point are considerably higher while the turbulence peak occurs at a shorter distance downstream of the downstream patch. In general, when the dense or medium patch is located at the upstream position, they have similar influence on TKE along the axis in between the patches and the profiles overlap to a large degree for all cases (Fig. 13d–f). The placement of the sparse patch at the upstream position leads to lower TKE and the peak occurs farther downstream from the patches.

When considering two solid cylinders in staggered arrangement, the spacing tested herein for the staggered configuration ($L/D = 3.5$ and $T/D = 1.5$) constitutes a boundary, albeit at a slightly lower Re_D of 20000, between the immediate unification of the wakes of the two cylinders into a single wake or the occurrence of two separate cylinder wakes with individually developed vortices [58]. The two patches in staggered configuration analyzed in the present study form two separate wakes and exhibit a tendency to merge at the downstream (Fig. 8), similar to the side-by-side patches (Fig. 10). The two wakes appear to merge at a shorter distance when the density of the patches is increased, while the density of the neighboring upstream patch affects the wake of the downstream patch mostly at its side that is closer to the longitudinal axis between the patches at $y/D = 0$. When compared to side-by-side patches, transverse turbulence in the wake of staggered patches remains fairly elevated at $10D$ downstream of the downstream patch and is relatively similar to that observed behind an isolated patch of same density.

Contrary to the side-by-side configuration, a denser neighboring patch (i.e., the upstream patch) in the staggered configuration induced the lower velocities throughout the longitudinal axis in between the patches, including the section close to the patches, until the two patch wakes merged into one (Fig. 11d–f). The reason for this is that the wakes of the two patches begin to interact at a shorter distance when the upstream patch is denser (Fig. 8a). Flow through an isolated dense patch recovers at a shorter distance and generates more patch scale turbulence compared to flow through an isolated sparse patch [20]. This fact in combination with the flow that is diverted from the downstream patch towards the wake of the upstream patch may explain the faster mixing and the lower centerline velocities that are observed, despite the enhanced flow contraction owed to the increased density of the upstream patch.

Cornacchia et al. [49] highlighted the importance of turbulence in patches with different densities in staggered configuration. In their flume experiment, they observed that when a patch of vegetation with denser and taller canopy (*Callitriche*) was placed upstream of a patch with sparser and shorter canopy (*Groenlandia*) the ammonium uptake rates were increased for both of them, compared to the opposite configuration. This was due to the fact that the dense patch at the upstream was exposed to higher mean flow velocities while the sparse patch at the downstream was benefited from the turbulence that was advected from the dense patch. As a result, understanding the interaction between patches with different densities is imperative not only for patches of same species with varying density but also for the interaction and coexistence of different species in a heterogeneous aquatic environment.

4 Conclusions

Neighboring vegetation patches affect each other's flow pattern, nutrient availability, and scour pattern. While a few recent studies have analyzed the effect of spacing between two vegetation patches on the flow field, the wake of two patches with different densities has not been thoroughly investigated yet. To this end, the present experimental study analyzed the flow pattern in the wake of two neighboring patches of emergent vegetation with combinations of three different patch densities (solid volume fractions equal to 0.059, 0.114, and 0.188). The patches were tested in side-by-side ($L/D = 0$ and $T/D = 1.5$) and staggered ($L/D = 3.5$ and $T/D = 1.5$) arrangements. The most notable differences were observed in the wake of the upstream patch in staggered configuration, which was significantly shortened due to flow diversion induced by the downstream patch, with the density of the latter influencing the mean velocities in the wake. In addition, the presence of the downstream patch distorted the von Karman vortex street that is otherwise observed downstream of an isolated patch. On the contrary, the mean velocities in the wake of the downstream patch in staggered configuration or in the wake of a patch in side-by-side configuration were hardly affected by the presence of a neighboring patch and both wakes were similar to the wake of an isolated patch with same density. However, TKE was significantly elevated in the near wake region of the sparse patch when it was placed in the downstream position of the staggered arrangement. This can potentially maintain sediment in suspension and inhibit the longitudinal expansion of the patch. The flow pattern downstream of two side-by-side patches with dissimilar densities was characterized by two asymmetric patch wakes with a jet stemming from in between the patches, the momentum of which dissipated at different rate at each of its sides. The wakes of the two patches interacted and eventually formed a single large wake with minimum velocity and suppressed turbulence at the axis in between the patches, which can potentially favor propagule entrapment and the establishment of seedlings for patch extension.

Acknowledgements Vasileios Kitsikoudis acknowledges financial support for postdoctoral research from The Scientific and Technological Research Council of Turkey—TUBITAK 2216 (Ref. No. 21514107-115.02-45898) and from Istanbul Technical University Scientific Research Projects Units (ITU-BAP)—Postdoctoral Research Support. The authors are grateful to Isilsu Yildirim and to ITU Hydraulics Laboratory technicians Mevlut Ulucinar, Hasan Yalcin, and Yasar Aktas for their assistance with the experiments.

References

1. Costanza R, d'Arge R, de Groot R, Farber S, Grasso M, Hannon B, Limburg K, Naeem S, O'Neill RV, Paruelo J, Raskin RG, Sutton P, van den Belt M (1997) The value of the world's ecosystem services and natural capital. Nature 387:253–260. https://doi.org/10.1038/387253a0
2. Dosskey MG, Vidon P, Gurwick NP, Allan CJ, Duval TP, Lowrance R (2010) The role of riparian vegetation in protecting and improving chemical water quality in streams. J Am Water Resour Assoc 46:261–277. https://doi.org/10.1111/j.1752-1688.2010.00419.x
3. Kemp JL, Harper DM, Crosa GA (2000) The habitat-scale ecohydraulics of rivers. Ecol Eng 16:17–29. https://doi.org/10.1016/s0925-8574(00)00073-2
4. Gran K, Paola C (2001) Riparian vegetation controls on braided stream dynamics. Water Resour Res 37:3275–3283. https://doi.org/10.1029/2000wr000203
5. Temmerman S, Bouma TJ, Van de Koppel J, Van der Wal D, De Vries MB, Herman PMJ (2007) Vegetation causes channel erosion in a tidal landscape. Geology 35:631–634. https://doi.org/10.1130/g23502a.1
6. Kearney WS, Fagherazzi S (2016) Salt marsh vegetation promotes efficient tidal channel networks. Nat Commun 7:12287. https://doi.org/10.1038/ncomms12287
7. Schwarz C, Gourgue O, van Belzen J, Zhu Z, Bouma TJ, van de Koppel J, Ruessink G, Claude N, Temmerman S (2018) Self-organization of a biogeomorphic landscape controlled by plant life-history traits. Nat Geosci 11:672–677. https://doi.org/10.1038/s41561-018-0180-y
8. Larsen LG (2019) Multiscale flow-vegetation-sediment feedbacks in low-gradient landscapes. Geomorphology 334:165–193. https://doi.org/10.1016/j.geomorph.2019.03.009
9. Wright K, Hiatt M, Passalacqua P (2018) Hydrological connectivity in vegetated river deltas: the importance of patchiness below a threshold. Geophys Res Lett 45:10416–10427. https://doi.org/10.1029/2018gl079183
10. Montgomery JM, Bryan KR, Horstman EM, Mullarney JC (2018) Attenuation of tides and surges by mangroves: contrasting case studies from New Zealand. Water 10:1119. https://doi.org/10.3390/w10091119
11. Nepf HM (2012) Flow and transport in regions with aquatic vegetation. Annu Rev Fluid Mech 44:123–142. https://doi.org/10.1146/annurev-fluid-120710-101048
12. Nepf HM (2012) Hydrodynamics of vegetated channels. J Hydraul Res 50:262–279. https://doi.org/10.1080/00221686.2012.696559
13. Kitsikoudis V, Kibler KM, Walters LJ (2020) In-situ measurements of turbulent flow over intertidal natural and degraded oyster reefs in an estuarine lagoon. Ecol Eng 143:105688. https://doi.org/10.1016/j.ecoleng.2019.105688
14. Champion PD, Tanner CC (2000) Seasonality of macrophytes and interaction with flow in a New Zealand lowland stream. Hydrobiologia 441:1–12. https://doi.org/10.1023/a:1017517303221
15. Palmer MA, Bernhardt ES, Allan JD, Lake PS, Alexander G, Brooks S, Carr J, Clayton S, Dahm CN, Shah JF, Galat DL, Loss SG, Goodwin P, Hart DD, Hassett B, Jenkinson R, Kondolf GM, Lave R, Meyer JL, O'Donnell TK, Pagano L, Sudduth E (2005) Standards for ecologically successful river restoration. J Appl Ecol 42:208–217. https://doi.org/10.1111/j.1365-2664.2005.01004.x
16. Beechie TJ, Sear DA, Olden JD, Pess GR, Buffington JM, Moir H, Roni P, Pollock MM (2010) Process-based principles for restoring river ecosystems. Bioscience 60:209–222. https://doi.org/10.1525/bio.2010.60.3.7
17. Vargas-Luna A, Crosato A, Anders N, Hoitink AJ, Keesstra SD, Uijttewaal WS (2018) Morphodynamic effects of riparian vegetation growth after stream restoration. Earth Surf Process Landf 43:1591–1607. https://doi.org/10.1002/esp.4338
18. Kibler KM, Kitsikoudis V, Donnelly M, Spiering DW, Walters L (2019) Flow–vegetation interaction in a living shoreline restoration and potential effect to mangrove recruitment. Sustainability 11:3215. https://doi.org/10.3390/su11113215
19. Takemura T, Tanaka N (2007) Flow structures and drag characteristics of a colony-type emergent roughness model mounted on a flat plate in uniform flow. Fluid Dyn Res 39:694–710. https://doi.org/10.1016/j.fluiddyn.2007.06.001
20. Chen Z, Ortiz A, Zong L, Nepf H (2012) The wake structure behind a porous obstruction and its implications for deposition near a finite patch of emergent vegetation. Water Resour Res 48:W09517. https://doi.org/10.1029/2012wr012224
21. Zong L, Nepf H (2012) Vortex development behind a finite porous obstruction in a channel. J Fluid Mech 691:368–391. https://doi.org/10.1017/jfm.2011.479

22. Yagci O, Tschiesche U, Kabdasli MS (2010) The role of different forms of natural riparian vegetation on turbulence and kinetic energy characteristics. Adv Water Resour 33:601–614. https://doi.org/10.1016/j.advwatres.2010.03.008
23. Yagci O, Celik MF, Kitsikoudis V, Kirca VSO, Hodoglu C, Valyrakis M, Duran Z, Kaya S (2016) Scour patterns around isolated vegetation elements. Adv Water Resour 97:251–265. https://doi.org/10.1016/j.advwatres.2016.10.002
24. Schoelynck J, Creëlle S, Buis K, De Mulder T, Emsens WJ, Hein T, Meire D, Meire P, Okruszko T, Preiner S, Gonzalez RR, Silinski A, Temmerman S, Troch P, Oyen TV, Verschoren V, Visser F, Wang C, Wolters JW, Folkard A (2018) What is a macrophyte patch? Patch identification in aquatic ecosystems and guidelines for consistent delineation. Ecohydrol Hydrobiol 18:1–9. https://doi.org/10.1016/j.ecohyd.2017.10.005
25. Sukhodolov AN, Sukhodolova TA (2010) Case study: effect of submerged aquatic plants on turbulence structure in a lowland river. J Hydraul Eng 136:434–446. https://doi.org/10.1061/(asce)hy.1943-7900.0000195
26. Kitsikoudis V, Yagci O, Kirca VSO, Kellecioglu D (2016) Experimental investigation of channel flow through idealized isolated tree-like vegetation. Environ Fluid Mech 16:1283–1308. https://doi.org/10.1007/s10652-016-9487-7
27. Nicolle A, Eames I (2011) Numerical study of flow through and around a circular array of cylinders. J Fluid Mech 679:1–31. https://doi.org/10.1017/jfm.2011.77
28. Chang K, Constantinescu G (2015) Numerical investigation of flow and turbulence structure through and around a circular array of rigid cylinders. J Fluid Mech 776:161–199. https://doi.org/10.1017/jfm.2015.321
29. Follett EM, Nepf HM (2012) Sediment patterns near a model patch of reedy emergent vegetation. Geomorphology 179:141–151. https://doi.org/10.1016/j.geomorph.2012.08.006
30. Ortiz AC, Ashton A, Nepf H (2013) Mean and turbulent velocity fields near rigid and flexible plants and the implications for deposition. J Geophys Res Earth Surf 118:2585–2599. https://doi.org/10.1002/2013jf002858
31. Yagci O, Yildirim I, Celik MF, Kitsikoudis V, Duran Z, Kirca VSO (2017) Clear water scour around a finite array of cylinders. Appl Ocean Res 68:114–129. https://doi.org/10.1016/j.apor.2017.08.014
32. Green JC (2005) Comparison of blockage factors in modelling the resistance of channels containing submerged macrophytes. River Res Appl 21:671–686. https://doi.org/10.1002/rra.854
33. Nikora V, Larned S, Nikora N, Debnath K, Cooper G, Reid M (2008) Hydraulic resistance due to aquatic vegetation in small streams: field study. J Hydraul Eng 134:1326–1332. https://doi.org/10.1061/(asce)0733-9429(2008)134:9(1326)
34. Bal K, Struyf E, Vereecken H, Viaene P, De Doncker L, de Deckere E, Mostaert F, Meire P (2011) How do macrophyte distribution patterns affect hydraulic resistances? Ecol Eng 37:529–533. https://doi.org/10.1016/j.ecoleng.2010.12.018
35. Luhar M, Nepf HM (2013) From the blade scale to the reach scale: a characterization of aquatic vegetative drag. Adv Water Resour 51:305–316. https://doi.org/10.1016/j.advwatres.2012.02.002
36. Cornacchia L, Folkard A, Davies G, Grabowski RC, Koppel J, Wal D, Wharton G, Puijalon S, Bouma TJ (2019) Plants face the flow in V formation: a study of plant patch alignment in streams. Limnol Oceanogr 64:1087–1102. https://doi.org/10.1002/lno.11099
37. Gurnell A (2014) Plants as river system engineers. Earth Surf Process Landf 39:4–25. https://doi.org/10.1002/esp.3397
38. Jones CG, Lawton JH, Shachak M (1994) Organisms as ecosystem engineers. Oikos 69:373–386. https://doi.org/10.2307/3545850
39. Bouma TJ, van Duren LA, Temmerman S, Claverie T, Blanco-Garcia A, Ysebaert T, Herman PMJ (2007) Spatial flow and sedimentation patterns within patches of epibenthic structures: combining field, flume and modelling experiments. Cont Shelf Res 27:1020–1045. https://doi.org/10.1016/j.csr.2005.12.019
40. Schoelynck J, de Groote T, Bal K, Vandenbruwaene W, Meire P, Temmerman S (2012) Self-organised patchiness and scale-dependent bio-geomorphic feedbacks in aquatic river vegetation. Ecography 35:760–768. https://doi.org/10.1111/j.1600-0587.2011.07177.x
41. Sumner D (2010) Two circular cylinders in cross-flow: a review. J Fluids Struct 26:849–899. https://doi.org/10.1016/j.jfluidstructs.2010.07.001
42. Zhou Y, Alam MM (2016) Wake of two interacting circular cylinders: a review. Int J Heat Fluid Flow 62:510–537. https://doi.org/10.1016/j.ijheatfluidflow.2016.08.008
43. Vandenbruwaene W, Temmerman S, Bouma TJ, Klaassen PC, de Vries MB, Callaghan DP, van Steeg P, Dekker F, van Duren LA, Martini E, Balke T, Biermans G, Schoelynck J, Meire P (2011)

Flow interaction with dynamic vegetation patches: implications for biogeomorphic evolution of a tidal landscape. J Geophys Res 116:F01008. https://doi.org/10.1029/2010jf001788
44. Meire DWSA, Kondziolka JM, Nepf HM (2014) Interaction between neighboring vegetation patches: impact on flow and deposition. Water Resour Res 50:3809–3825. https://doi.org/10.1002/2013wr015070
45. Kondziolka JM, Nepf HM (2014) Vegetation wakes and wake interaction shaping aquatic landscape evolution. Limnol Oceanogr Fluids Environ 4:106–119. https://doi.org/10.1215/21573689-2846314
46. de Lima PHS, Janzen JG, Nepf HM (2015) Flow patterns around two neighboring patches of emergent vegetation and possible implications for deposition and vegetation growth. Environ Fluid Mech 15:881–898. https://doi.org/10.1007/s10652-015-9395-2
47. Yamasaki TN, de Lima PH, Silva DF, Preza CGA, Janzen JG, Nepf HM (2019) From patch to channel scale: the evolution of emergent vegetation in a channel. Adv Water Resour 129:131–145. https://doi.org/10.1016/j.advwatres.2019.05.009
48. van Wesenbeeck BK, van de Koppel J, Herman PMJ, Bouma TJ (2008) Does scale-dependent feedback explain spatial complexity in salt-marsh ecosystems? Oikos 117:152–159. https://doi.org/10.1111/j.2007.0030-1299.16245.x
49. Cornacchia L, Licci S, Nepf H, Folkard A, Wal D, Koppel J, Puijalon S, Bouma TJ (2019) Turbulence-mediated facilitation of resource uptake in patchy stream macrophytes. Limnol Oceanogr 64:714–727. https://doi.org/10.1002/lno.11070
50. Thomas RE, Schindfessel L, McLelland SJ, Creëlle S, Mulder TD (2017) Bias in mean velocities and noise in variances and covariances measured using a multistatic acoustic profiler: the Nortek Vectrino Profiler. Meas Sci Technol 28:075302. https://doi.org/10.1088/1361-6501/aa7273
51. Mori N, Suzuki T, Kakuno S (2007) Noise of acoustic Doppler velocimeter data in bubbly flows. J Eng Mech 133:122–125. https://doi.org/10.1061/(asce)0733-9399(2007)133:1(122)
52. Goring DG, Nikora VI (2002) Despiking acoustic Doppler velocimeter data. J Hydraul Eng 128:117–126. https://doi.org/10.1061/(asce)0733-9429(2002)128:1(117)
53. Wahl TL (2003) Discussion of "Despiking acoustic Doppler velocimeter data" by D.G. Goring and V.I. Nikora. J Hydraul Eng 129:484–487. https://doi.org/10.1061/(asce)0733-9429(2003)129:6(484)
54. Pope SB (2000) Turbulent flows. Cambridge University Press, Cambridge
55. Sumer BM, Fredsoe J (1997) Hydrodynamics around cylindrical structures, advanced series on ocean engineering, vol 12. World Scientific, Singapore
56. Kitsikoudis V, Kirca VSO, Yagci O, Celik MF (2017) Clear-water scour and flow field alteration around an inclined pile. Coast Eng 129:59–73. https://doi.org/10.1016/j.coastaleng.2017.09.001
57. Lee JHW, Chu VH (2003) Turbulent jets and plumes: a Lagrangian approach. Springer US, New York. https://doi.org/10.1007/978-1-4615-0407-8
58. Wong CW, Zhou Y, Alam MM, Zhou TM (2014) Dependence of flow classification on the Reynolds number for a two-cylinder wake. J Fluids Struct 49:485–497. https://doi.org/10.1016/j.jfluidstructs.2014.05.008